JOURNAL OF MATERIALS SCIENCE 26 (1991) 1919–1930

The fracture morphology of fast unstable fracture in polycarbonate

C. M. AGRAWAL, G. W. PEARSALL
Department of Mechanical Engineering and Materials Science, Duke University, Durham, NC 27706, USA

Fracture tests were conducted on polycarbonate using compact tension specimens. With the aid of fractographic analysis techniques the effects of various geometric and test parameters on the fracture-surface morphology were studied. Four distinct regions were identified on the fracture surface: (i) initiation region, (ii) mist region, (iii) mirror region, and (iv) banded region. The extent of the mist region was found to depend inversely on the ratio of the initial crack length, a, and the specimen width, W. The fracture morphology also was affected by changes in the test temperature and externally applied compressive loads, but it did not exhibit any significant trends as a function of the loading rate. A qualitative model, called the "critical thickness craze crack interaction" (CCI) model, was developed to explain the micromechanisms involved in the fracture process. This model is based on the proposition that the various features on the fracture surface are generated by the interaction of the crack with a critical thickness craze, where the latter is that part of the main craze which has a thickness greater than some critical thickness, d.

1. Introduction

Fractographic analysis of a fracture surface can yield valuable information about the microstructure of the material, the fracture mechanisms, and whether the fracture was ductile or brittle. Fractography has been used extensively to establish structure–property–failure relationships for metals. With the advent of synthetic structural polymers like polycarbonate, fractography is becoming an important tool in understanding the strength and failure of engineering plastics. For example, fracture morphology can be used to determine crack initiation sites, direction of crack propagation, and mode of crack formation. The degree of roughness of a polymeric fracture surface can be associated generally with the amount of energy expended in the fracture process [1]. Also the appearance of the surface often can be quantitatively related to the crack velocity [2]. An analysis of the fracture-surface morphology of polycarbonate should lead to insights into the energy-consuming micromechanical events occurring during the fracture process. In order to gain insights that could eventually lead to a comprehensive understanding of the toughness of polycarbonate, the present research was undertaken to study the micromechanisms responsible for the fracture morphology produced by unstable fast fracture in this engineering plastic.

2. Background information

Perhaps the most distinctive feature of the micromechanics of deformation in polymers, when compared to metals and inorganic glasses, is their long-chain molecular structure, which permits them to craze. There is fairly universal agreement now that crazes play an important role in the fracture of glassy polymers. In such polymers, fracture involves the formation and subsequent rupture of crazes. Crazes serve as crack nucleation sites as well as precursors to cracks [3–10]. Under stress, crazes grow by drawing additional material from the craze–bulk polymer interface into the craze volume [4, 11–14]. As a craze thickens, voids develop along the centreline of the craze and also along the craze–bulk interface [3].

Fractures through crazes have been reported to proceed by one of two mechanisms.

1. Fibrils along the centreline of the craze fail by necking and snap back to the matrix surface on either side, leaving a layer of crazed material easily detectable by optical fractography [15].

2. Fibrils fail at the craze–matrix interface. This process leaves only one matrix surface with a layer of craze material at that location. The crack frequently jumps from one interface to the other [15–17] producing characteristic patterns of bands on the fracture surfaces.

In a very detailed study of the brittle fracture of polycarbonate, primarily in impact, Hull and Owen [18] divided each resulting fracture surface into four different regions: initiation, mist, mirror and banded.

2.1. Initiation region

Initially in the initiation region the crack grows by tearing crazes [16, 19], and the ruptured fibrils snap back to the craze surface creating a rough surface [20, 21]. Lee *et al.* [20] have characterized the region as a river pattern, formed due to the crazes simultaneously developing on different planes and then interacting. Unstable crack growth ultimately takes place

0022–2461/91 $03.00 + .12

preferentially in one of these crazes [18]. The extent of the initiation region in the direction of crack travel has been determined to be in the range 150–270 μm for notched impact specimens [18] and approximately 500 μm for tensile specimens [16, 17].

2.2. Mist region

The mist region follows the initiation region and appears hazy to the naked eye. This region consists of truncated protrusions and depressions [16] with "islands" of protruding material on one fracture surface matching the "islands" of recessed material on the other and vice versa [18]. This appearance may be the result of the crack oscillating between the two craze–matrix interfaces [15–17]. Sometimes a banded structure is noticed superimposed on the island structure in the mist region and is attributed to the effect of an interaction between the propagating crack front and elastic waves generated by the fracture [15].

2.3. Mirror region

The mirror region is an optically smooth area interrupted occasionally by elongated closed loops, called here "conical" markings (roughly elliptical but elongated with the major axis parallel to the direction of crack travel) which are associated with a step change in the plane of crack propagation. The interaction of the crack front with secondary fractures that initiate ahead of it and on planes parallel but slightly removed from its plane are presumably responsible for these conical shapes. Each conical marking has a well-defined focus [22]. Andrews [23] has mathematically predicted the shape of related parabolic markings found on the surface of poly-methylmethacrylate (PMMA).

2.4. Banded region

The fourth region described by Hull and Owen [18] follows the mirror region and consists of evenly spaced, well-defined, parallel bands with some substructure of unknown origin. These bands, which are hereafter referred to as "end bands", have also been observed on the fracture surface of polycarbonate by others [16, 24]. Bands similar in some respects have been reported for polystyrene [15, 25]. According to Ravetti *et al.* [24] each band consists of two regions: the first region has areas with evidence of pulled out material, the second region has no marks and has a fine granular texture. The occurrence of banded structures on the fracture surface of other polymeric materials also has been reported widely [2, 15–17, 22, 25–30].

3. Experimental procedure

3.1. Specimen preparation

The material used in this research was General Electric Company's LEXAN® brand bisphenol-A polycarbonate. The material was supplied as extruded sheets in a nominal thickness of 12.7 mm. The primary specimen geometry used in this study was the compact tension specimen (CTS) as shown in Fig. 1 [31]. However, single-edge notch (SEN) specimens also were tested. These SEN specimens were prepared per approximate specifications provided by Knott [32].

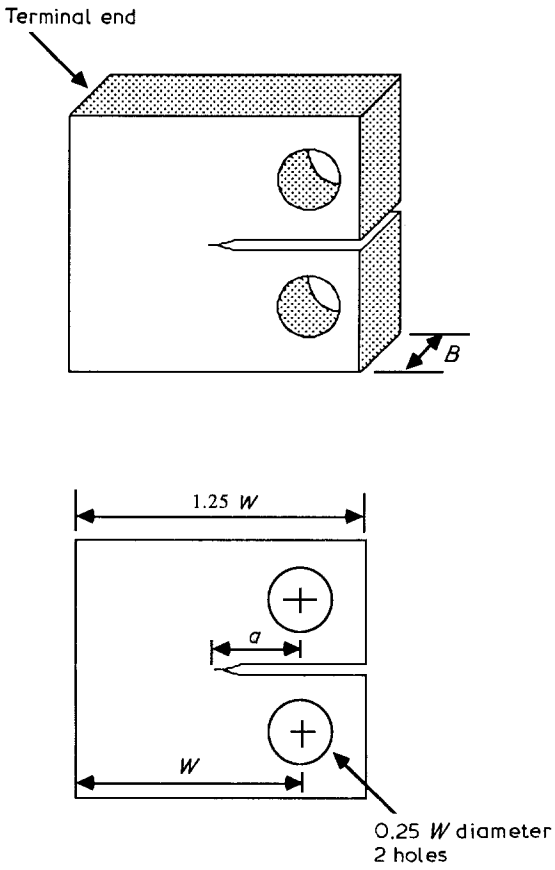

Figure 1 Compact tension specimen.

Because polymers are prone to developing multiple crazes and to undergoing material orientation in fatigue, fatigue precracking techniques commonly used for metals were not considered in this study. Instead a new technique was developed [33–35] to introduce a precrack at the base of the machined notch of the specimen as shown in Fig. 2. This was accomplished in three stages, described below.

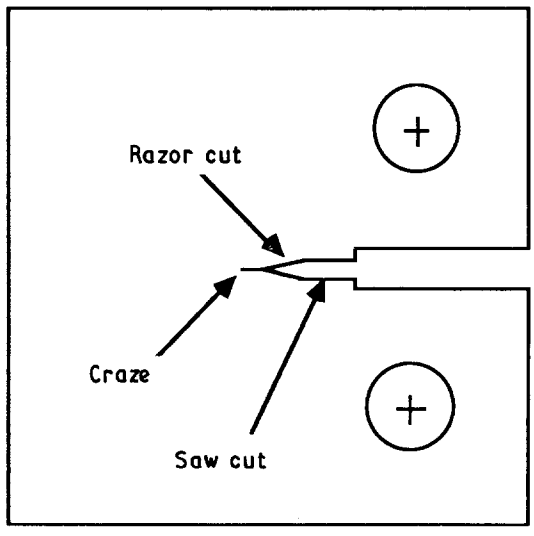

Figure 2 Precrack in the compact tension specimen.

1. A cut was made at the mid-line of the notch using a jewellers saw with an extra-fine blade (no. 2/0, thickness approximately 0.25 mm).

2. The saw cut then was deepened using a razor blade. A sawing action was used to avoid causing molecular orientation.

3. Next the specimen was loaded in an Instron tensile testing machine. Using a hypodermic needle and a syringe, a small amount (0.015 ml) of an ethyl alcohol–water solution was introduced at the tip of the razor cut. The specimen was then loaded at a slow crosshead speed of 0.05 mm min^{-1} until a craze appeared at the tip of the razor cut, at which time the load was released. Crazes have a refractive index different from that of the bulk material, and so appear silvery, which makes them easy to detect visually in a transparent polymer.

The use of ethanol (ethyl alcohol) as a crazing agent for polycarbonate avoids the problems that may accompany fatigue precracking [35]. However, ethanol is a crazing agent and may plasticize the polycarbonate. To avoid the possibility of the ethanol adversely affecting the measurement of fracture toughness, each specimen was rinsed in a stream of distilled water immediately after crazing and then was subjected to evacuation for 24 h in a vacuum chamber (10^{-4}–10^{-5} torr (1.333×10^{-2}–1.333×10^{-3} Pa)) to remove any residual ethanol and moisture.

3.2. Fracture tests

The fracture tests were carried out in an Instron tensile testing machine. The specimens were tested at a machine crosshead speed of 25.4 mm min^{-1}. Fracture toughness values were computed as per the outline given in ASTM standard E399-83 for metals [31]. Fracture tests on SEN specimens were conducted both under tensile and three-point-bend loading conditions. Tests were also performed to study the effects of a compressive load on the terminal or back end of the specimen (Fig. 1) during the fracture test. This compressive load was applied in a direction parallel to the tensile load that was applied by the testing machine. A C-clamp in conjunction with a calibrated force gauge was used to apply the compressive load.

In order to ascertain the effects of temperature on the fracture morphology, some fracture tests were conducted at elevated temperatures. These tests were performed in a convective electric furnace with a capacity to generate and control temperatures from 23 °C to approximately 205 °C. The furnace was mounted in the testing frame of the tensile testing machine, and the elevated temperature fracture tests were conducted *in situ*. Tests were performed at six different temperature levels ranging from approximately 23 °C to approximately 80 °C.

Fracture tests also were conducted at different loading rates by varying the machine crosshead speed of the tensile testing machine in the range 12.7 to 254.0 mm min^{-1}.

3.3. Post-fracture examination

The fracture surface was examined initially in a stereo microscope with a magnification range of × 6.6– × 40. A reflected/transmitted light microscope (× 50–× 600) with a camera attachment was used to take optical photographs of the surface morphology. For examining the details of the fracture surface at higher magnifications, the surface was vacuum sputter-coated with approximately 0.03 μm gold-palladium and examined in a scanning electron microscope.

4. Results

4.1. Fracture morphology

The fracture surfaces of most specimens were found to have four distinct regions: a rough initiation region, a mist region, then a smooth mirror-like region with elongated conical markings, and finally a region of end bands. On examination under a microscope the initiation region always showed thick remnants of craze material (see Fig. 3). The mist region comprised small islands of protruding or recessed material, the recesses on one fracture surface mating with the protrusions on the opposite fracture surface (Figs 4 and 5). Figs 6–11 illustrate a typical transition of morphology along the crack path in the mist region on the fracture surface of polycarbonate. A banded structure can be seen to be superimposed on the pattern of these "islands" (Fig. 9). In the transition zone between the mist and the mirror regions these bands disintegrate, and elongated islands are formed as shown in Fig. 11. The mirror region comprises a relatively featureless background with conical markings superimposed (Figs 12 and 13). A step change in the crack plane provides the boundary of each conical marking. Near the terminal end (back edge) of the fracture surface the mirror region abruptly changes to yield a banded structure which shows vestiges of craze material (see Figs 14 and 15). These end bands were observed not only on the terminal end of the fracture surface but also were formed immediately prior to crack arrest on those specimens that did not experience complete fracture.

4.2. Specimen dimensions and test parameters

In order to investigate the effects of the specimen dimensions on the fracture morphology, specimens

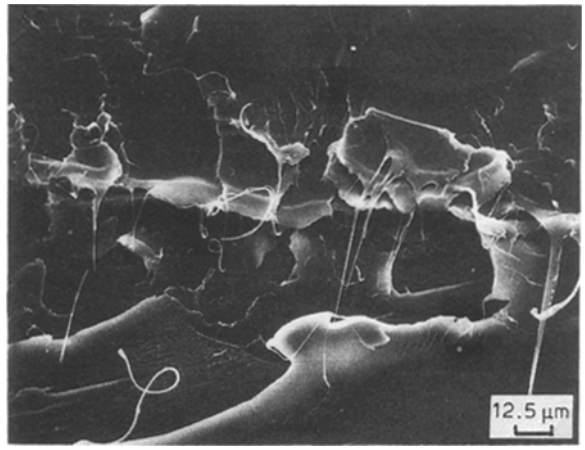

Figure 3 Rough surface of crack initiation region showing broken fibrils.

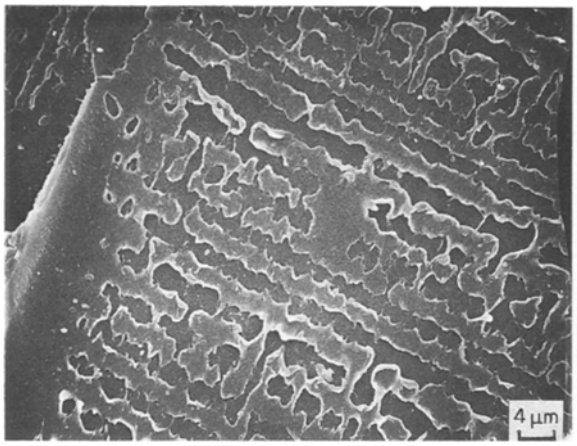

Figure 4 Protrusions and recesses in the mist region. Protrusions on this surface mate with the recesses on fracture surface shown in Fig. 5.

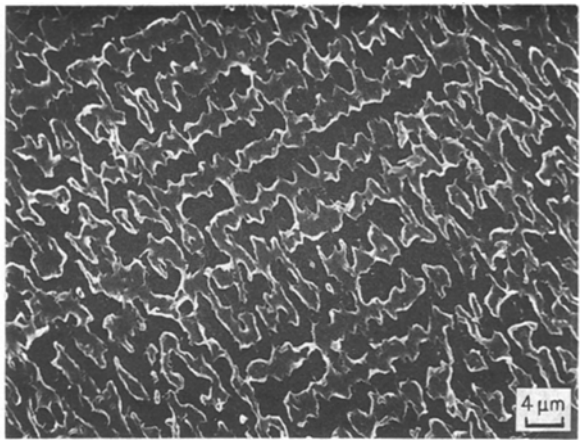

Figure 7 Island structure and start of fine band development in the mist region. Crack propagation direction: lower right to upper left corner.

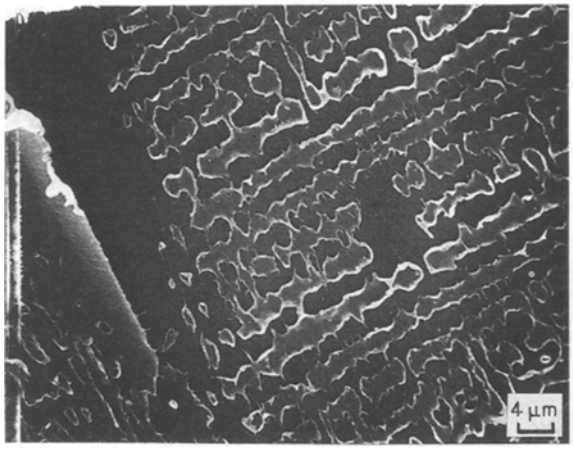

Figure 5 Portrusions and recesses in the mist region. Protrusions on this surface mate with the recesses on fracture surface shown in Fig. 4.

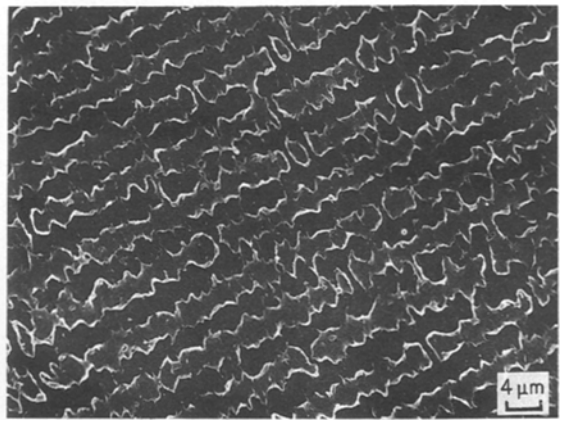

Figure 8 Continuation of fine band development in the mist region. Crack propagation direction: lower right to upper left corner.

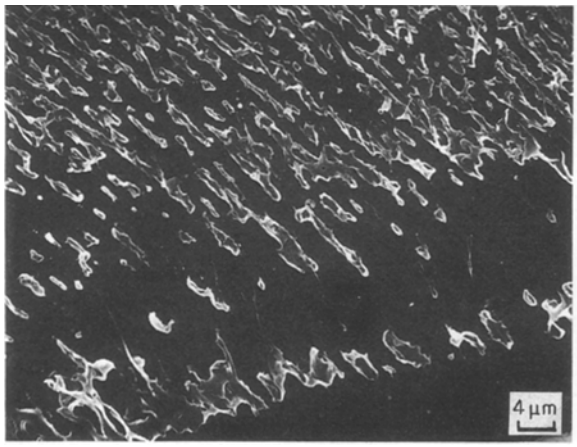

Figure 6 Start of the mist region. Crack propagation direction: lower right to upper left corner.

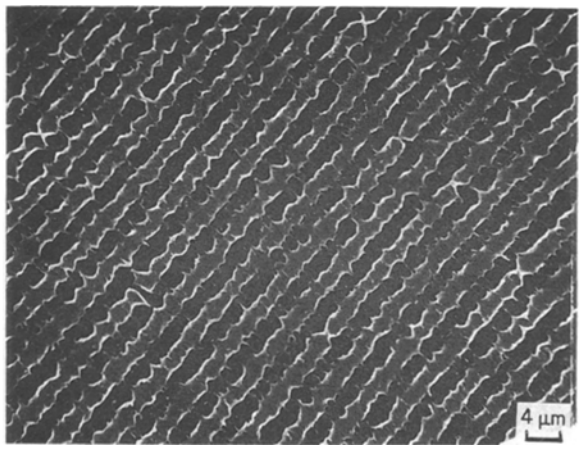

Figure 9 Fine bands fully developed in the mist region. Crack propagation direction: lower right to upper left corner.

with different widths, W, and initial crack lengths, a, were tested. The extent of the mist region was found to increase with decreasing a/W ratios. However, individually neither a nor W had any significant effect on the fracture morphology for a constant a/W ratio.

The extent of the mist region showed an increasing trend with increasing test temperatures as shown in Fig. 16. In addition the fracture toughness increased slightly with increasing test temperature [35]. The fracture morphology did not exhibit any significant

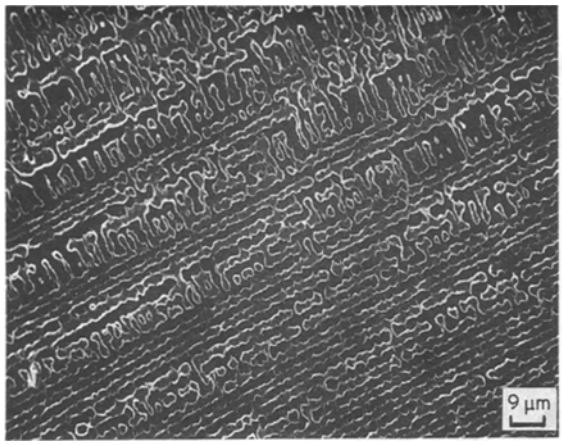

Figure 10 Fine bands disintegrating into islands in the mist region. Crack propagation direction: lower right to upper left corner.

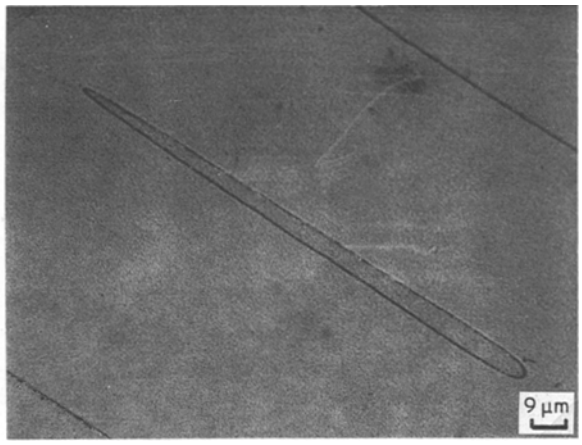

Figure 13 Single conical section. Crack propagation direction: lower right to upper left corner.

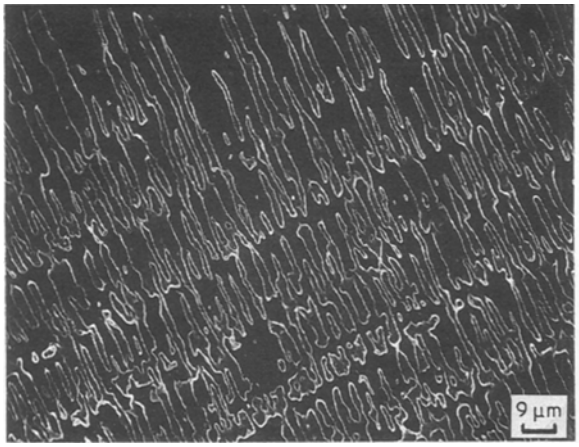

Figure 11 Transition between mist region and mirror region. Crack propagation direction: lower right to upper left corner.

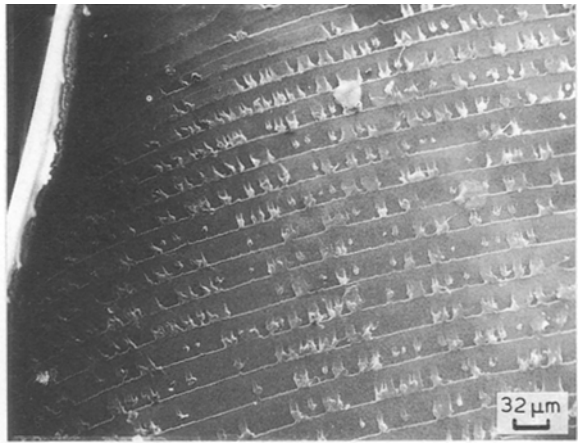

Figure 14 End-wall bands. Crack propagation direction: bottom to top.

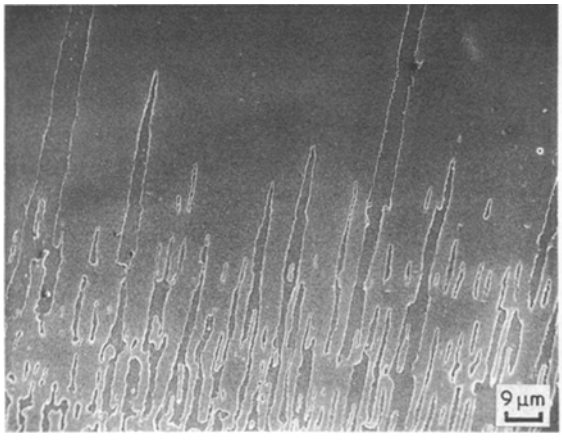

Figure 12 Conical sections at start of mirror region. Crack propagation direction: bottom to top.

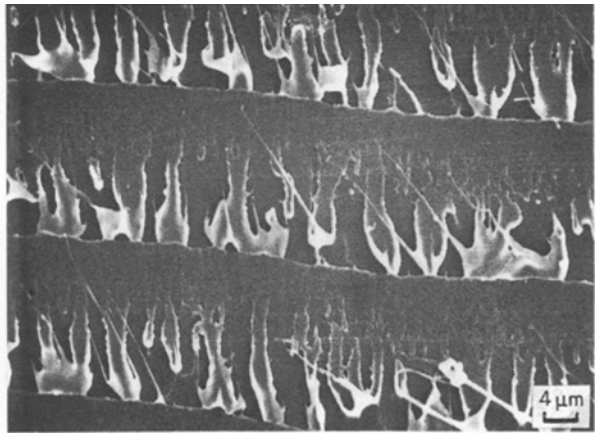

Figure 15 End-wall bands showing two regions in each band. Crack propagation direction: bottom to top.

differences with changes in the loading rate but the fracture toughness exhibited a strong decreasing trend with increasing loading rate [35].

Compressive loads applied close to the terminal end of the specimen during the tensile fracture test had a significant effect on the fracture morphology. The area of the end bands showed a slight increase with increasing compressive loads as shown in Fig. 17. Also, the distance between the tip of the precrack and start of the end bands was a decreasing function of the

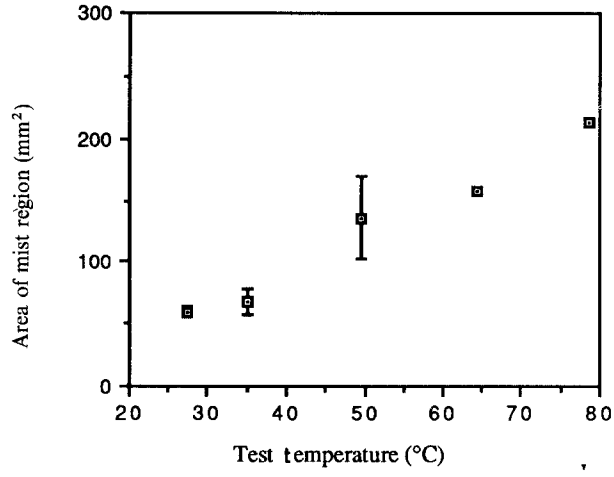

Figure 16 Effect of test temperature on area of mist region.

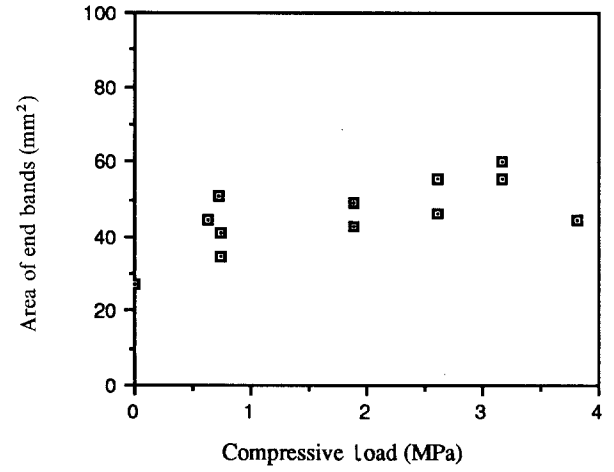

Figure 17 Area of end bands as a function of compressive load on terminal end of the specimen.

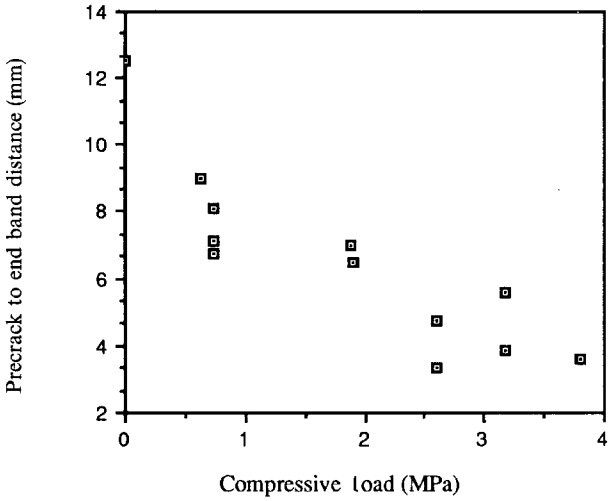

Figure 18 Relationship between external compressive load on terminal end of specimen and distance between tip of precrack and start of the end band region.

compressive loads (Fig. 18). In all cases the crack was arrested approximately at the mid-point of the section loaded in compression by the C-clamp.

To assess further the effect of bending-induced compressive stresses on the fracture morphology, SEN specimens were tested in tension and in bending. End bands were absent from the fracture surface of SEN specimens tested in tension. For the SEN specimens ($a/W = 0.5$) tested using three-point bend loading, the end bands covered approximately 52% of the fracture surface. End bands covered approximately 10%–15% of the fracture surface for the case of CTS with similar a/W ratios tested in tension.

5. Discussion

5.1. Crack initiation region

After fracture, the crack initiation region on the fracture surface shows a very rough texture with evidence of extensive crazing and bulk material drawing. Often the material in the craze is drawn from the bulk in the form of large fibrils, remnants of which are found on the surface (Fig. 3). The rough surface is indicative of crazes having formed on several planes close to one other. Upon further craze growth, the material separating the adjacent crazes is sheared, leaving behind "flaps" of material on the surface. Earlier studies also have presented evidence for the existence of several crazes in the initiation region [20, 21]. According to Hull and Owen, unstable crack growth takes place preferentially in one of these crazes [18].

The results of this study indicate that the extent of the crack initiation craze correlates very well with the measured fracture toughness (Fig. 19). The initiation region is the site of intense crazing by drawing of fibrils from the matrix followed by subsequent crack growth by craze tearing. The combined process of craze formation and slow crack growth in the initiation region is a relatively high energy-consuming process. Thus a greater extent of the crack initiation craze would consume more energy, and this would be reflected in a higher measured value of fracture toughness. The extent of this crack initiation craze would be expected to be greater when the precrack did not act as an efficient crack initiator and additional crazing was required in order to initiate a crack.

It has been established that crazes are the precursors of cracks in polymers [3–8]. Crazing always

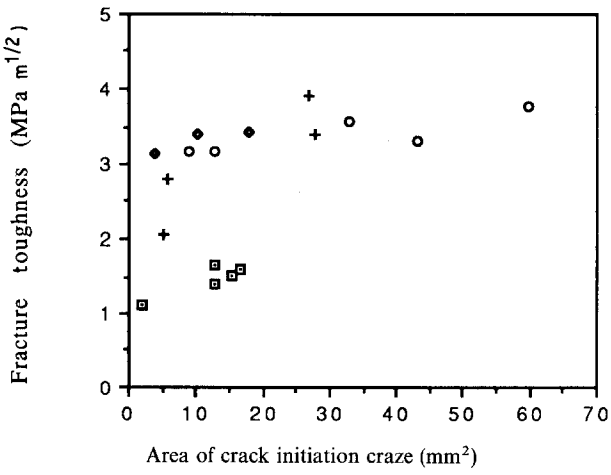

Figure 19 Relationship between fracture toughness and extent of crack initiation craze. Crosshead speed (mm min^{-1}): (⊡) 254.0, (+) 127.0, (○) 50.8, (◆) 25.4.

precedes the crack, not only prior to the onset of fast fracture, but also during the fast propagation itself. Empirical evidence for this hypothesis can be obtained from studies that have photographically recorded the presence of crazes ahead of cracks [11, 36]. The propagation of a craze preceding crack propagation would be preferred thermodynamically because the process of drawing material from the bulk polymer during crazing would consume less energy than required for the bond breaking involved in crack propagation. In addition, during crack propagation work is required to impart kinetic energy to the two fracture surfaces in order to move them apart. This energy would be in addition to that required for bond breaking. By contrast, during crazing the two bulk–craze interfaces are still connected via fibrils and as a consequence their relative displacement would be much less than that of the two fracture surfaces. Thus an energy-based criterion for craze propagation would be expected to be satisfied before a similar criterion for fast crack propagation is satisfied. Such criteria have been developed both for craze and crack propagation [37]. The relative rates and extents of propagation of crazes and cracks, however, would depend on several parameters, including the stress distribution in the specimen.

5.2. Mist region

The extent of the mist region was observed in this study to increase with decreasing precrack length and increasing test temperature. Simultaneous with this increase in the mist region there was also an increase in the fracture stress values. It is possible that the increase in the mist is related to the increase in the magnitude of the tensile stress in the specimen. Also, for a fixed loading rate, a higher fracture stress entails a corresponding longer time to fracture. An increase in the time to fracture would be expected to give more time for a craze to grow both in thickness and length. Keeping these observations in perspective, a model was developed to explain the fracture morphology in the mist region.

5.2.1. Critical thickness craze crack initiation (CCI) model

As a result of slow growth in the initiation region, the craze grows to a critical length which then satisfies an energy-based criterion for fast growth. The transition from slow to fast craze propagation also will mark the change from the initiation to mist regions on the fracture surface. At this point the crack still would not have reached the critical length required to trigger catastrophic propagation and hence would be expected to lag behind the craze. By the time the crack enters a mode of fast propagation through the craze, the craze would have had time to grow in thickness. As shown in Fig. 20, two craze fronts can be visualized: (1) the main craze front, and (2) the critical thickness craze front where the critical thickness craze is that part of the main craze which has a thickness greater than some critical thickness, d (Fig. 21). It is

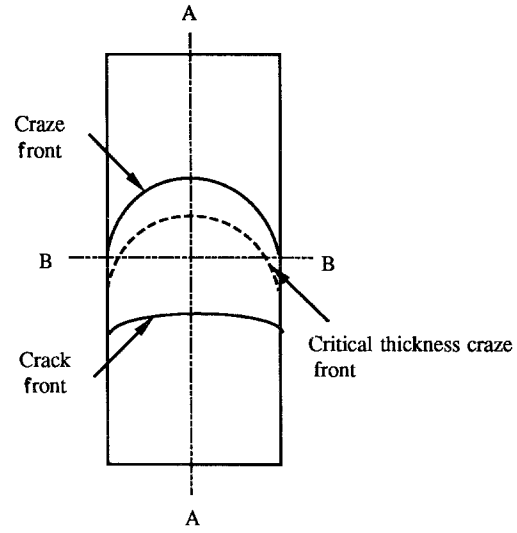

Figure 20 Schematic representation of the craze, critical thickness craze, and crack fronts.

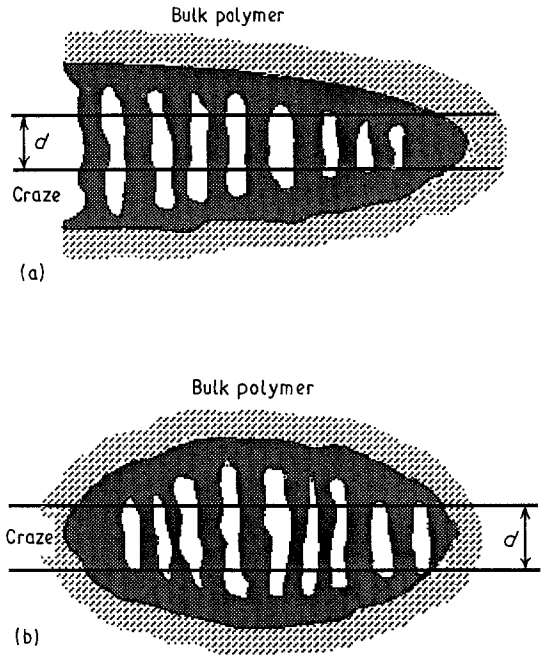

Figure 21 Schematic representation of cross-sections through a craze showing minimum thickness, d, required for generation of mist region. (a) Section AA from Fig. 20. (b) Section BB from Fig. 20.

proposed here that the fine detail within the mist region is dependent on the craze thickness and is formed only when the crack propagates through a craze with a thickness greater than d. In other words, the mist is formed only when the critical thickness craze and crack interact. Owing to the lack of plane strain constraint and hence low hydrostatic tensile stresses at the side surfaces of the specimen, the craze thickness is minimal in these regions and would normally be below the critical thickness. Hence, this model predicts that the crack would propagate through this thin layer of crazed material without leaving a rough surface in its wake. This argument is supported by the inspection of the mist region on the fracture surface

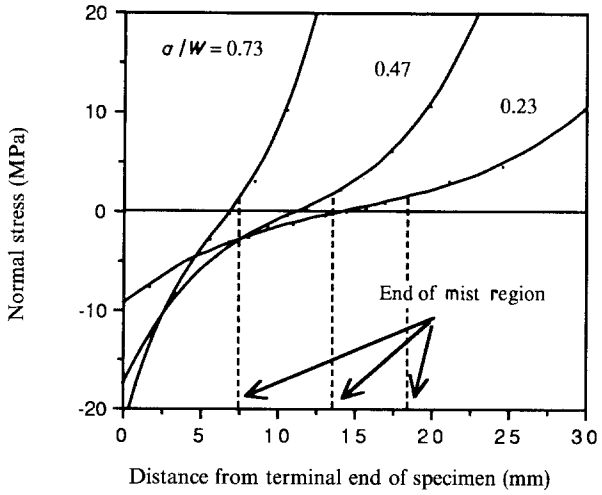

Figure 22 Stress distribution for three a/W ratios.

which reveals mirror regions adjacent to the side surfaces of the specimen.

In order to approximate the static stress distribution present in the specimen prior to crack propagation, a finite element analysis was conducted. The stress distributions obtained for three specimens with a/W ratios in the range 0.22–0.73 are shown in Fig. 22. Owing to the bending moment generated by the geometry of the CTS, the stress normal to the crack plane is not constant over the ligament length but has a gradient: the stress is tensile at the tip of the crack and compressive at the terminal end of the specimen. As the craze and crack grow, the initial stress distributions change so that the stress at the craze tip becomes positive (tensile). However, because of its viscoelastic nature, the material cannot adjust to the changes instantaneously with the result that the tensile stress ahead of the craze front is effectively reduced due to the lingering effects of the compressive stress. As the terminal end of the specimen is approached the effects of the compressive stress increase, leading to a decrease in the tensile stress and consequently a decrease in the craze velocity. It is known that a critical stress level or crazing stress is required to produce crazing [38]. When the tensile stress decreases to below the crazing stress, the craze hesitates while the stress once again starts to increase due to the viscoelastic adjustments in the material. At this point the crack front starts to overtake the critical thickness craze front, resulting in a change from mist to mirror. As a result, the crack would now be propagating through a craze that has a thickness less than the critical thickness required for a rough mist region to form. Thus, according to this "critical thickness craze crack interaction" (CCI) model, there will be a change in the morphology from a rough fracture surface to one that is relatively featureless: the mirror region. Also, after the crazing stress has been re-established at the craze tip, it is possible that under certain conditions the craze might increase in velocity and once again the critical thickness craze front might overtake the crack front to yield another mist region after a short segment of the mirror region. A second mist region has been observed on several specimens, especially those with long specimen widths. However, the specific conditions that generate the second mist have not yet been identified conclusively.

5.2.2. Extent of mist region

The end of the first mist region measured from the terminal end of the specimen is shown in Fig. 22 for three a/W ratios. As shown in this figure the static levels at these points lie in the range 1.50–1.88 MPa. A similar analysis for a SEN specimen yielded a stress value of 1.66 MPa. It should be noted that due to the dynamic nature of the problem the static stress distributions are not strictly valid. However, the actual stresses experienced by the craze at this point would be a function of the static stress. The relatively small variation in the static stress values at the end of the first mist, even when measured over a wide range of a/W ratios, gives credence to the concept of a critical stress that determines the end of the first mist.

The extent of the furthest reaches of the mist (end of second mist region if two mist regions existed) were measured for a set of specimens with a/W ratios in the range 0.22–0.73. Using a finite element analysis the static stress gradients at the end of the total mist region were computed. The extent of the mist and the inverse of the stress gradient show very similar slopes when plotted against the a/W ratio (Fig. 23).

The similarity in the trends exhibited by the extent of the mist and the inverse of the stress gradient might be a manifestation of the effects of the compressive stresses. A higher stress gradient implies that the craze front encounters the effects of the compressive stress after travelling only a small distance, resulting in a short mist region. The stress gradients will be determined in part by the a/W ratio. The maximum stress at the crack tip prior to crack propagation is approximately the same for all a/W ratios tested. Hence the stress gradient will depend on the length of the uncracked ligament, $W(1 - a/W)$, for a fixed width W. For high a/W ratios the stress gradients will be higher and vice versa. This is reflected in the relationship between the extent of mist and the a/W ratio as shown in Fig. 23. Small a/W ratios corresponding to long

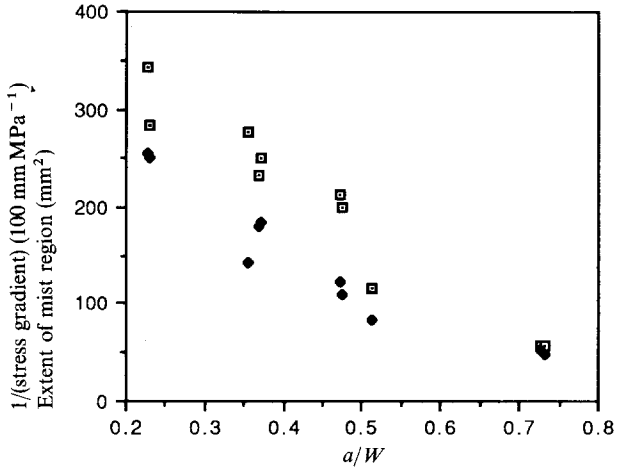

Figure 23 Variation of stress gradient and extent of mist area with a/W ratio. ⊡ Extent of mist, ◆ 1/Stress gradient.

uncracked ligaments and low stress gradients lead to large mist regions. On the other hand, large a/W ratios correspond to short uncracked ligament lengths that result in high stress gradients and small mist regions.

If the formation of the mist region is dependent on the relative positions of the crack and critical thickness craze fronts as postulated by the CCI model, then any parameter which modifies these relative positions would also be expected to modify the extent of the mist. It has been reported in earlier studies that elevated temperatures enhance crazing [15, 39]. The crazing stress decreases with increasing temperature [40], and hence a longer segment of the specimen would be expected to undergo crazing before the stress in the craze tip falls below the critical crazing stress. Also, these higher temperatures should impede brittle fracture because the yield strength of the material decreases with increasing temperatures, facilitating local deformation. Thus increased test temperatures would be expected to increase the relative distance between the crack front and the critical thickness craze front. This increase would result in extra time for more of the craze to attain the critical effective thickness required for generating the mist region when the crack propagates through the craze. Thus, the extent of the mist region would increase with increasing temperatures. This hypothesis is supported by the results of those experiments in this study that were devised to study the effects of the testing temperature on the fracture of polycarbonate. The extent of the mist region did exhibit a strong trend with increasing testing temperature as shown in Fig. 16.

5.2.3. Mist substructures

Within the mist region a fine banded structure is observed (Fig. 9). These bands consist of strips of crazed material. The protrusions on one fracture surface correspond to depressions on the other and vice versa. The band spacing was estimated to be approximately 9 μm. This spacing does not change with changes in the test conditions or specimen geometry. It is suggested that these fine bands are generated by the crack jumping from one craze–bulk interface to the other due to stress perturbations caused by fibrils in the craze breaking and snapping back on the interfaces. This is shown graphically in Fig. 24. Suppose fibril A breaks at location X and snaps back like a broken rubber band on to interface 2. The resulting impact on the interface could cause an increase in the tensile stress (in fibril B) at location Y causing failure to initiate there. Fibril B then would snap back and impact interface 1 causing fibril C to break at Z. This process would lead to a banded topography.

Superimposed on the bands in the mist region, another set of bands was detected (Fig. 25). The spacing for these superimposed bands was determined to be approximately 35 μm. These bands imparted a shallow, barely noticeable waviness to the surface. Each superimposed band consisted of two sub-bands: the first of these sub-bands comprised the fine band structure already described. In the second sub-band the fine bands tended to disintegrate into an island

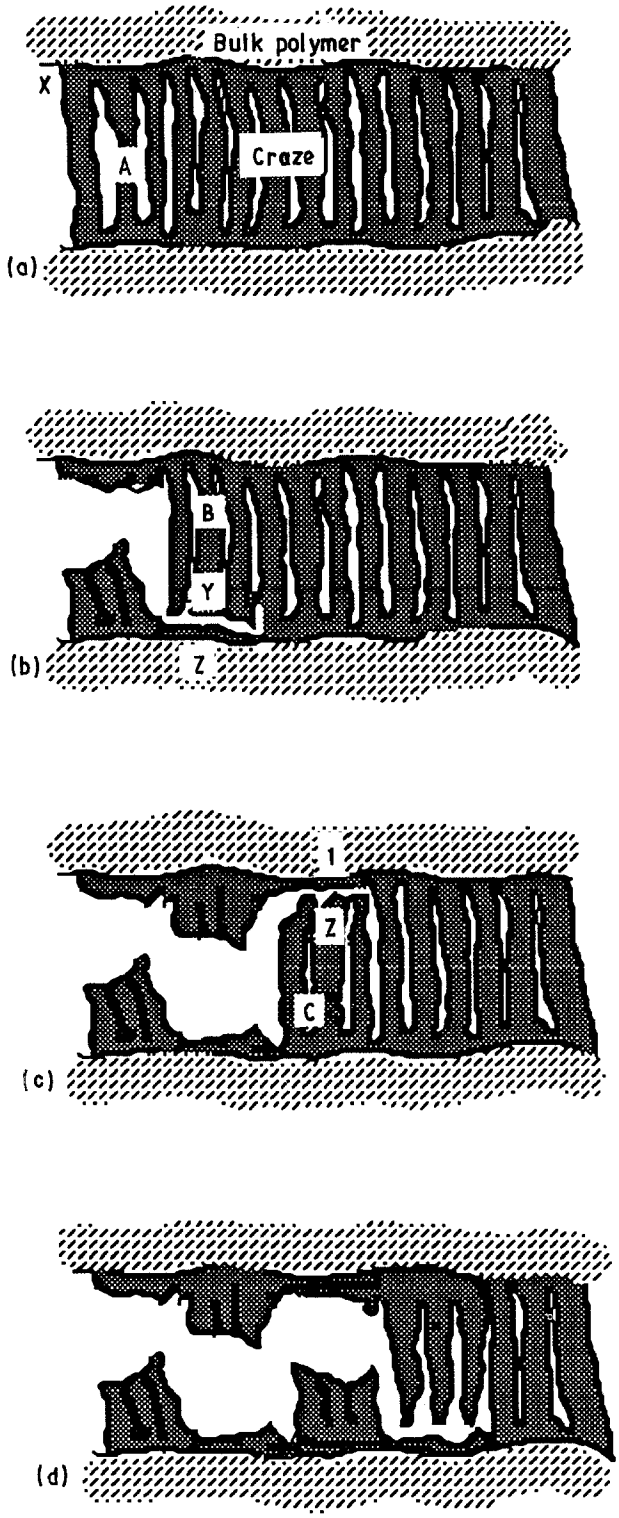

Figure 24 "Rubber band" model for formation of fine bands.

structure. The source/cause of these superimposed bands is not known definitely. However, it is possible that they are the result of the interaction of the crack front with an elastic wave propagating through the material. The start of the brittle fracture in polycarbonate is accompanied by a loud sound. An elastic wave in the polycarbonate certainly could generate an audible sound wave in the surrounding air.

5.2.4. Shape of the mist region

According to the CCI model, the final shape of the mist region prior to its transition to the mirror region

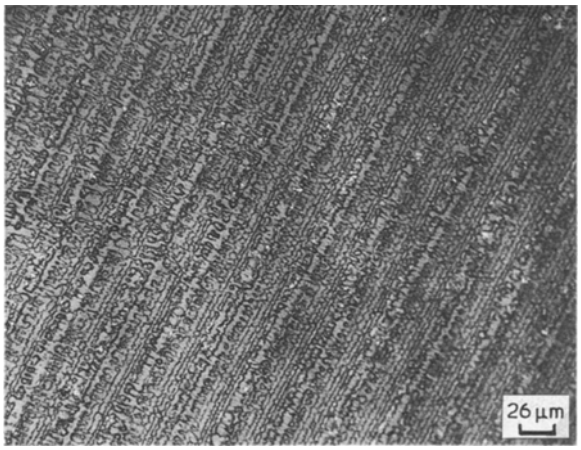

Figure 25 Superimposed bands in mist region.

will be determined by the shapes and relative positions of the craze and crack fronts. The craze front, which is in the shape of an arc, starts to lose speed as it encounters a decreasing stress. On the other hand, there is evidence that the crack front for fast brittle fracture is parabolic in shape at the transition from slow to fast fracture [41]. It would be expected that to some degree this shape would be retained by the crack as it propagates through the craze. As the crack front nears the decelerating craze front, it overtakes the critical thickness craze front at the sides and centre of the specimen (Fig. 26). Like the craze, and for the same reasons, the crack is decelerating at this stage. Also, because the crack front is now very close to the craze front it would tend to lose its curvature and conform

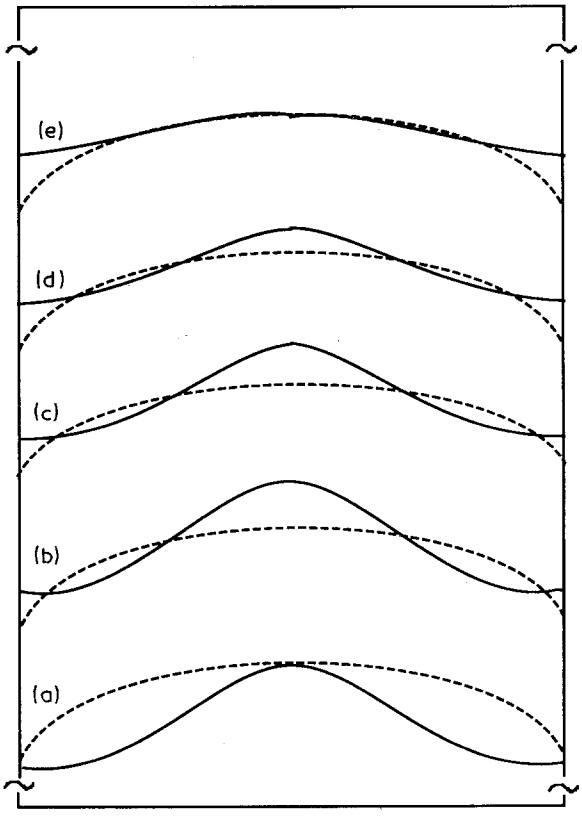

Figure 26 Proposed interaction between (——) crack front and (– – –) critical thickness craze on fracture surface of CTS of polycarbonate.

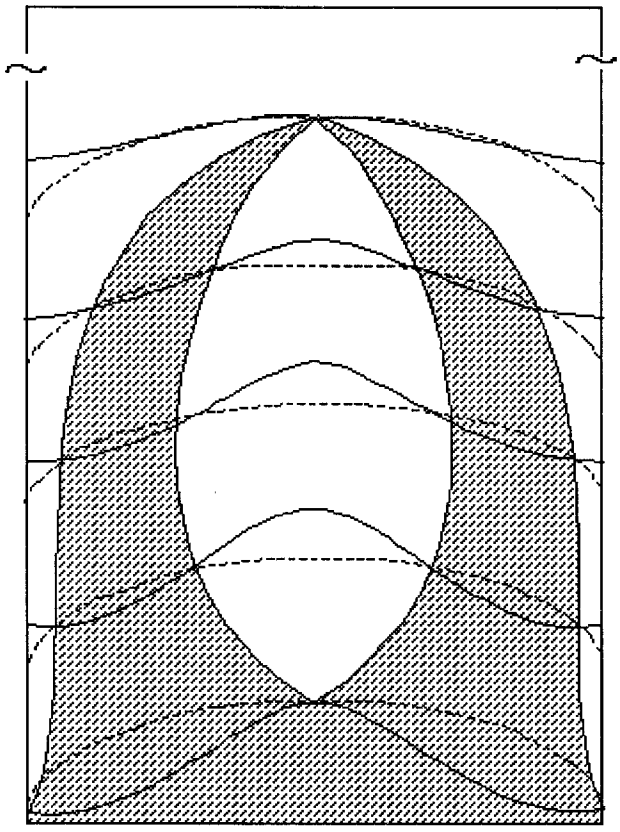

Figure 27 Generation of the crescent-like shapes on fracture surface of CTS of polycarbonate. (– – –) critical thickness craze; (——) crack; shaded area, mist region.

to the shape of the craze front. The velocity of the craze may once again tend to increase because the viscoelastic material may adjust to the applied stress resulting in the re-establishment of the critical crazing stress at the craze tip. This sequence would lead to the formation of crescent-shaped mist regions (Fig. 27) observed on the fracture surface of polycarbonate.

5.3. Mirror region

The region immediately following the mist region is the mirror region. This region has an optically featureless surface with a random distribution of elongated conical sections. The featureless, shiny, mirror region is possibly the result of the crack closely following the craze front. In this configuration the craze does not have sufficient time to grow in thickness with the result that when the crack propagates through it, a relatively smooth fracture surface is generated. The conical sections observed on the fracture surface are generated when the main crack front interacts with secondary cracks which initiate ahead of the main crack. The conical sections (Fig. 13) are closed at both ends and therefore are different from those described by Andrews [23], which were parabolic in shape. In his analysis, Andrews assumed constant velocities for both the main and secondary cracks. This assumption leads to parabolic or elliptical shapes, depending on the velocities. However, in the present study it was determined that closed eccentric, elliptic, conical shapes seen in polycarbonate can be generated theoretically using Andrews' analysis if there is a decrease in

the velocity of the main crack relative to the velocity of the secondary crack. This result was obtained by schematically reconstructing the generation of the elongated conical shapes on a graph.

As the crack length increases and the crack and craze fronts approach the non-crack end of the specimen, their velocities will decrease rapidly. This decrease is due primarily to two reasons: (i) the stress in the specimen decreases as the crack length increases because the testing machine is unable to keep pace with the crack and cannot maintain a constant load; (ii) the initial compressive stress generated in the specimen by the bending moment is maximum at the terminal end of the specimen (Fig. 22). It is likely that the velocity of the secondary crack also decreases, although maybe not at the same rate. The closed conical shapes will be generated only when the main crack is travelling much faster than the secondary crack front at the time the secondary crack initiates and there is a decrease in the velocity of the main crack relative to the secondary crack.

As the stress continues to decrease it ultimately falls below the critical crazing stress at some point near the non-crack end of the specimen. This decrease causes the craze to stop propagating momentarily and marks the abrupt transition from the mirror region to the end band region.

5.4. End bands

The mirror region is followed by the fourth and final region on the fracture surface: end bands. These bands are different (Figs 14 and 15) in appearance from those seen within the mist region. Each band is approximately 35 μm wide and comprises two regions: the first half shows "flaps" of craze material and evidence of material drawing and tearing. The second half is relatively featureless but sometimes exhibits faint traces of an "island" structure. The band width of the end bands was found to be invariant with the changes in test conditions investigated here.

The end bands also were formed prior to crack arrest in those specimens in which the crack failed to propagate all the way to the terminal end of the specimen. Kambour *et al.* [42] have reported the formation of a "set of ridges" prior to crack arrest in the case of double cantilever beam specimens. It appears likely that the end bands observed here are generated under conditions where the crack velocity is decreasing.

It is proposed that these end bands are formed due to a "stick–slip" type of mechanism [16, 18, 26]. As a result of the decreasing tensile stress in the mirror region, the craze slows down and finally, unable to grow any further, it comes to a stop, thus marking the end of the mirror region. This momentary stop provides the crack front with enough time to reach the craze front and conform to its shape. The merging of the crack and craze fronts increases the stress on the material ahead of the common front and causes the craze to grow once more. However, due to the low tensile stress in this part of the specimen the craze does not grow substantially and again comes to a halt. Once again the crack propagates through the new craze, thereby increasing the stress on the material ahead of the craze. This process repeats itself either until the crack reaches the end of the specimen or until the stress decreases to a level which is too low for further craze or crack propagation. According to the present model the width of each band is a measure of the craze growth during one cycle of this mechanism.

The effect of compressive stress on the end bands was studied by loading the terminal end of the specimen in compression during fracture tests. The results indicate that there is a slight increase in the extent of end bands with increasing compressive loads (Fig. 17). However, it was also determined that increasing the compressive stress resulted in a decrease in the distance between the precrack and the first end band (Fig. 18). This early start of the end bands may be due to the compressive stresses reducing the effective tensile stress to a level below the critical value required for crazing. This reduction would be expected to cause the craze to stop momentarily while the crack grows and the stress re-establishes itself. As outlined above, this process would generate a banded structure.

In an attempt to investigate further the role of compressive stresses on the formation of end bands, SEN specimens were tested both in tension and under three-point bend loading conditions. The SEN specimens tested in tension have a lower compressive stress due to a smaller bending moment than a CTS of comparable size. On the other hand, SEN specimens tested under three-point bend testing conditions have much higher maximum compressive stresses. The results of this study indicate that no end bands are formed on the fracture surface of SEN specimens tested in tension, while the fracture surface of specimens tested under three-point bend testing conditions exhibited extensive regions of end bands. An attempt was also made to reduce the compressive stress in compact tension specimens, using epoxy to fix a 1:6 mm thick plate of aluminium to the terminal end of the specimen. Owing to the higher stiffness of the metal, the compressive stress in the polycarbonate should decrease. No end bands were formed on the fracture surface of such specimens, thus further validating the hypotheses that these bands are formed due to the damping effect which compressive stresses have on craze and crack propagation.

6. Conclusions

Fast, unstable fracture in polycarbonate generates a fracture surface morphology that can be subdivided into four distinct regions: an initiation region, a mist region, a mirror region, and an end-band region. At room temperature the plane strain fracture toughness, K_{Ic}, tends to increase with an increase in the extent of the initiation region but does not correlate with the extents of the other three regions of the fracture surface.

At room temperature, the extent of the mist region is inversely dependent on the a/W ratio over the range tested in this study, even though K_{Ic} is independent of a/W over this same range. However, for a constant

a/W ratio the mist region does not exhibit any dependence on either a or W individually.

Varying the loading rate by changing the crosshead speed of the tensile testing machine in the range 12.7–254.0 mm min^{-1} results in a corresponding decrease in the measured fracture toughness of polycarbonate but does not affect its fracture morphology. However, both K_{Ic} and the extent of the mist region increase with increasing test temperature.

An increase in axial compressive stress applied close to the terminal end (back edge) of the CTS during a fracture test results in a corresponding increase in the extent of the end bands and a decrease in the distance between the precrack and the first end band. A sufficiently high compressive stress can stop the crack before it propagates through the CTS.

Acknowledgements

The authors thank General Electric Co. for providing the LEXAN used in this study, and Becton Dickinson Co. for the use of their equipment. The contributions of Elizabeth Pittman to this work also are acknowledged.

References

1. A. T. DiBENEDETTO and K. L. TRACHTE, *J. Appl. Polym. Sci.* **14** (1970) 2249.
2. W. DÖLL, *J. Mater. Sci.* **10** (1975) 935.
3. D. HULL, in "Deformation and Fracture of High Polymers" (Plenum Press, New York, 1973) p. 171.
4. N. VERHEULPEN-HEYMANS, *Polymer* **20** (1979) 356.
5. J. G. WILLIAMS and G. P. MARSHALL, in "Deformation and Fracture of High Polymers" (Plenum Press, New York, 1973) p. 557.
6. R. J. MORGAN and J. O'NEAL, *Polym. Engng Sci.* **18** (1978) 1081.
7. E. J. KRAMER and E. W. HART, *Polymer* **25** (1984) 1667.
8. W. G. KNAUSS, *Appl. Mech. Rev.* **26** (1973) 1.
9. R. P. KAMBOUR and R. E. BARKER, *J. Polym. Sci. A2*, **4** (1966) 359.
10. R. N. HAWARD, B. M. MURPHY and E. F. T. WHITE, *ibid.* **9** (1971) 801.
11. T. CHAN, A. M. DONALD and E. J. KRAMER, *J. Mater. Sci.* **16** (1981) 676.
12. C. J. G. PLUMMER and A. M. DONALD, *J. Polym. Sci. B* **27** (1989) 325.
13. A. M. DONALD and E. J. KRAMER, *J. Mater. Sci.* **16** (1981) 2977.
14. E. PASSAGLIA, *Polymer* **25** (1984) 1727.
15. J. MURRAY and D. HULL, *J. Polym. Sci. A2* **8** (1970) 583.
16. R. J. MORGAN and J. E. O'NEAL, *Polymer* **20** (1979) 375.
17. R. J. MORGAN and J. E. O'NEAL, *J. Polym. Sci. Polym. Phys. Ed* **14** (1976) 1053.
18. D. HULL and T. W. OWEN, *ibid.* **11** (1973) 2039.
19. P. BEAHAN, M. BEVIS and D. HULL, *J. Mater. Sci.* **8** (1972) 162.
20. L. H. LEE, J. F. MANDELL and F. J. McGARRY, *Polym. Engng Sci.* **27** (1987) 1128.
21. J. MURRAY and D. HULL, *Polymer* **10** (1969) 451.
22. M. J. DOYLE, A. MARANCI, E. OROWAN and S. T. STORK, *Proc. R. Soc. London, Ser. A* **329** (1972) 137.
23. E. H. ANDREWS, "Fracture in Polymers" (Aberdeen University Press, London, 1968) p. 182.
24. R. RAVETTI, W. W. GERBERICH and T. E. HUTCHINSON, *J. Mater. Sci.* **10** (1975) 1441.
25. M. J. DOYLE, *ibid.* **10** (1975) 300.
26. R. P. KUSY and D. T. TURNER, *Polymer* **18** (1977) 391.
27. G. H. JACOBY, in "Electron Microfractography", ASTM STP 453 (American Society for Testing and Materials, Philadelphia, Pennsylvania, 1969) p. 147.
28. R. P. KUSY, H. B. LEE and D. T. TURNER, *J. Mater. Sci.* **11** (1976) 118.
29. A. P. GLOVER, F. A. JOHNSON and J. C. RADON, *Polym. Engng Sci.* **14** (1974) 420.
30. A. K. GREEN and P. L. PRATT, *Engng Fract. Mech.* **6** (1974) 71.
31. "Standard Method of Test for Plane Strain Fracture", ASTM E399-83, ASTM Annual Standards (American Society for Testing and Materials, Philadelphia, Pennsylvania, 1986).
32. J. F. KNOTT, in "Fundamentals of Fracture Mechanics" (Halsted Press, New York, 1979) p. 130.
33. L. E. PITTMAN, MS Thesis, Duke University, Durham (1985).
34. C. M. AGRAWAL and G. W. PEARSALL, in "Proceedings of the 14th International Symposium on Testing and Failure Analysis", Los Angeles, 1988 (ASM International, Metals Park, 1988) p. 405.
35. C. M. AGRAWAL and G. W. PEARSALL, submitted.
36. M. J. DOYLE, *J. Mater. Sci.* **10** (1975) 159.
37. C. M. AGRAWAL and G. W. PEARSALL. Unpublished research.
38. A. N. GENT, *J. Mater. Sci.* **5** (1970) 925.
39. O. K. SPURR and W. D. NIEGISCH, *J. Appl. Polym. Sci.* **6** (1962) 585.
40. A. M. DONALD, *J. Mater. Sci.* **20** (1985) 2630.
41. M. J. WERT, A. SAXENA and H. A. ERNST, *J. Testing Evaln* **18** (1990) 1.
42. R. P. KAMBOUR, A. S. HOLIK and S. MILLER, *J. Polym. Sci. Polym. Phys. Ed.* **16** (1978) 91.

Received 30 October 1989
and accepted 24 April 1990